



Exergy-based sustainability analysis of combined cycle gas turbine plant integrated with double-effect vapor absorption refrigeration system

Ashutosh Mishra¹ · B. B. Arora¹ · Akhilesh Arora¹

Received: 20 May 2023 / Accepted: 14 November 2023 / Published online: 11 December 2023
© The Author(s), under exclusive licence to The Brazilian Society of Mechanical Sciences and Engineering 2023

Abstract

The implementation of inlet air cooling in combined cycle gas turbine (CCGT) plant is imperative to mitigate the adverse consequences, such as reduced performance, caused by high ambient temperatures. Therefore, this paper presents a novel idea of integration of the CCGT plant and a double-effect water-LiBr vapor absorption refrigeration system for inlet air cooling. The absorption system utilizes the waste heat of CCGT exhaust gas to cool the ambient air at the compressor's inlet. The objective of this paper is to compare the energy, exergy, and sustainability factors of an integrated system to that of the standalone CCGT plant. This novel approach has improved the thermodynamic performance and environmental sustainability of the integrated system. Subsequently, the energy analysis reveals that maximum improvements in work output and thermal efficiency of 5.04% and 1.64%, respectively, have been reported. Furthermore, the results show that as the ambient temperature rises, the work output of the standalone CCGT system decreases faster than that of the integrated CCGT system. Also, the integrated plant is more exergetically efficient. The maximum yield in exergetic efficiency and total work output is observed at the degrees of cooling of 8 K and 18 K, respectively. Therefore, this system can be operated suitably within this range of degrees of cooling. Besides, the exergy-based sustainability indicators are found to be improved. The environmental sustainability index has increased by up to 3.52%, showing improved fuel utilization. This also indicates that, for the same amount of emissions, the integrated CCGT plant generates more power.

Keywords Combined cycle · Inlet air cooling · Exergy analysis · Vapor absorption · Sustainability indicators

List of symbols

m	Mass flow rate (kg/s)
h	Specific enthalpy (kJ/kg)
v	Specific volume (m ³ /kg)
s	Specific entropy(kJ/kg k)
T	Temperature (K)
P	Pressure (bar)
E	Exergy
C	Specific heat (kJ/kg k)
W	Work (kW)
Q	Heat (kW)
X	Concentration (%)

Subscripts

a	Air
f	Fuel
m	Mechanical
s	Steam
g	Gas
AC	Air compressor
CC	Combustion chamber
GT	Gas turbine
hp	High pressure
lp	Low pressure
isen	Isentropic
sh	Superheated
dea	Deaerator
cond	Condenser
cw	Cooling water
in/i	Entry
out/ex	Exit
cv	Control volume
ph	Physical

Technical Editor: Monica Carvalho.

✉ Akhilesh Arora
akhilesharora@dce.ac.in

¹ Department of Mechanical Engineering, Delhi Technological University, New Delhi, India

ch	Chemical
ss	Strong solution
ws	Weak solution
ms	Medium solution
evap	Evaporator
de	Double effect
ex	Exergy
fw	Feed water
0	Dead state
D	Destruction

Abbreviations

CCGT	Combined cycle gas turbine
CCGTV	Combined cycle gas turbine with double-effect vapor absorption system
CIT	Compressor inlet temperature
GTC	Gas turbine cycle
STC	Steam turbine cycle
HRSG	Heat recovery steam generator
IAC	Inlet air cooling
TIT	Turbine inlet temperature
VARs	Vapor absorption refrigeration system
HPG	High-pressure generator
LPG	Low-pressure generator
COP	Coefficient of performance
HPST	High-pressure steam turbine
LPST	Low-pressure steam turbine
HPD	High-pressure drum
LPD	Low-pressure drum
RH	Relative humidity
LHV	Lower heating value
BFP	Boiler feed pump
CEP	Condensate extraction pump
SP	Solution pump

Greek symbols

η	Efficiency
γ	Ratio of specific heats
φ	Fuel depletion ratio
ω	Specific humidity
Δ	Difference
γ	Specific heat ratio

1 Introduction

The ever-increasing demand for energy and the constant depletion of resources are driving a shift toward more efficient power generation. Combined cycle gas turbine (CCGT) power plants enhance the performance of simple gas turbine plants that utilize the fuel energy in an efficient way [5]. The efficiency of CCGT plants has been achieved by up to 64% [44]. Higher efficiency encompasses cheaper generation and fewer emissions. CCGT power plants are

designed to run on specific operating conditions to fetch maximum efficiency. Ambient temperature is one of those significant operating conditions [6]. Environmental conditions, on the other hand, are not always advantageous. As the ambient air temperature rises, the performance of gas turbine power plants decreases [2]. It is essential to mitigate the adverse effects of high ambient air temperature by cooling it before intake to the air compressor [24]. Several researchers performed studies to observe the impact of ambient temperature on the performance of CCGT.

Erdem and Sevilgen [13] examined the electricity generation rate of a gas turbine (GT) power plant based on varying ambient temperatures corresponding to seven different climate conditions. The electricity generation rate is reduced by 2.87–0.71% in hot regions. The same is improved by 0.27–10.28% when the temperature of the inlet air is decreased to 10 °C. Along with the ambient temperature, the performance in terms of entropy generation rate and power output is also affected by the turbine inlet temperature (TIT) and pressure ratio. Choudhary and Sanjay [7] analyzed an integrated GT with a solid oxide fuel cell on the basis of these parameters (TIT and pressure ratio). And, when analyzing only the gas turbine component, the minimum entropy generation occurred at TIT of 1650 K and pressure ratio of 20. Rai et al. [34] investigated the impact of increasing ambient temperature on the power output of a CCGT plant consisting of two gas turbines and a steam turbine. The study revealed a decline in the overall and individual turbine power outputs. De Sa and Al Zubaidy [8] endorsed an empirical relationship for GT power production capacity when ambient temperature differs from ISO conditions (1.01 bar, 15 °C, and RH = 60%) [6]. For every 1 K above ISO that the ambient temperature went up, the GT lost 0.1% of its thermal efficiency and 1.47 MW of gross power output. Ehyaei et al. [10] modeled a CCGT thermodynamically and investigated the effect of inlet fogging. By performing optimization simultaneously, net power output, 1st law, and 2nd law efficiencies were reported to be increased by 17.24, 3.6, and 3.5%, respectively, for three months (June to August) of warm weather.

Mohapatra and Sanjay [30] compared two techniques of inlet air cooling (IAC), i.e., evaporative cooling and vapor compression cooling. In comparison with evaporative IAC, vapor compression IAC increased GT plant-specific work and thermal efficiency by 18.4 and 4.18%, respectively, while evaporative IAC increased these factors by 10.48 and 4.18%, respectively. Baakeem et al. [4] performed a comparative study of various IAC technologies coupled with a GT power plant in Riyadh. The optimized cooling capacity and air temperature were found to be 36 kW/m³s⁻¹ and 8 °C, respectively. This study proposed a wet-cooled condenser coupled to a sub-cooling multistage compressor refrigeration

system and a single-effect water-LiBr vapor absorption refrigeration system (VARS).

Since compressors utilize electricity from power plants as input, VARS is a well-known alternative to vapor compression refrigeration systems [35]. Researchers suggested an extensive range of inexpensive heat sources to drive a VARS, including Geothermal and solar energy. Kadam et al. [19] analyzed and compared thermo-economically the vapor compression refrigeration (VCR) system, VARS, and their hybrids for district cooling applications. It was discovered that VARS has the highest exergetic efficiency among all configurations. In addition, the integration of VARS with renewable energy resources was found to reduce both the environmental impact and the total cost. Matjanov [26] analyzed three heat source schemes for VARS: gas turbine exhaust, HRSG waste gases, and solar energy. The utilization of gas turbine waste heat in the absorption chiller was not preferable owing to the reduction in CHP efficiency. The most effective scheme was operating an absorption chiller on HRSG waste gases if the temperature of HRSG exhaust increased beyond 120 °C.

Singh [38] investigated a CCGT power plant integrated with an ammonia-water VARS. The study revealed that for the same fuel consumption, the total work output, 1st law efficiency, and exergy efficiency improved by 2.8, 1.193, and 1.133%, respectively. Mohapatra and Sanjay [31] analyzed a 3-pressure level HRSG integrated CCGT power plant equipped with an aqua ammonia VARS. At higher ambient temperatures, the total exergy destruction of the combined cycle was noticed to be higher. Also, the effect of ambient relative humidity was reported to be negligible on the performance of several components of the CCGT power plant. Meraj et al. [27] investigated the effect of increasing ambient temperatures on the single-effect water-LiBr VARS. It was reported that as ambient temperature rises, the coefficient of performance (COP) decreases. Elberry et al. [12] examined a dual-pressure HRSG combined cycle power plant incorporated with a single-effect water-LiBr absorption chiller. This study suggested that the HRSG exhaust gas temperature lower than 122 °C is the best scenario to employ a single effect VARS. However, Kaushik and Arora [20] reported the COP of a double-effect water absorption chiller is 1.6 to 1.7 times that of a single-effect absorption chiller. Further, Talukdar and Gogoi [42] compared a vapor power cycle equipped with single-effect and double-effect water-LiBr VARS for HPG temperatures ranging from 120 to 150 °C. The double-effect VARS had a superior COP (i.e., 1.411) than the single-effect system, which had a COP of 0.809. Similarly, the combined system's exergetic efficiency was reported to be 35.23% for double-effect integration versus 35.19% for single-effect integration.

However, numerous works of literature discuss the study of CCGT performance improvement via inlet air cooling;

several gaps have been identified but have not yet been addressed. In order to address these gaps, the present analysis aims to undertake a unique approach, hence showcasing its novelty. The gaps and attempts to address them are listed below:

- (1) The prevailing approach in previous studies by Singh [38] and Mohapatra and Sanjay [31] has predominantly involved the utilization of an Ammonia-water based VARS for cooling the inlet air. Despite the fact that water-LiBr VARS exhibits greater suitability from a performance standpoint. Hence, this analysis employs a water-LiBr-based absorption system.
- (2) Even though the HRSG exhaust temperature typically ranges between 120 and 160 °C [18], most studies have focused on single-effect VARS (water-LiBr or ammonia-water). None of the researchers have utilized water-LiBr double-effect VARS, despite the fact that it has a higher COP than a single-effect system and can exploit the HRSG exhaust energy more efficiently. Therefore, double-effect type VARS has been considered in the present analysis.
- (3) Moreover, the dual-pressure HRSG-based CCGT plant has been analyzed with the incorporation of double-effect water-LiBr VARS. Thus, the apprehended thermodynamic system is novel.
- (4) The integrated CCGT system itself has not yet been analyzed. In addition to analyzing this system thermodynamically, a comparison of exergy-based sustainability is made to calculate the improvement of the new system in comparison with the standalone CCGT plant.

In this study, a thorough 1st law analysis is performed, followed by a 2nd law analysis of the CCGT both with and without inlet air cooling. Moreover, the performance of these two scenarios has been compared to analyze the effects of ambient air temperature. Furthermore, several exergy-based sustainability indicators are computed, and their effects have been discussed.

2 System description

The system considered for analysis is a CCGT power plant, i.e., a conjunction of a gas turbine cycle (GTC) and a steam turbine cycle (STC). GTC comprises an air compressor, a combustion chamber, and a gas turbine. The air is compressed and then directed to the combustor section, where it is mixed with fuel (i.e., natural gas). The hot gas that results from the combustion chamber is guided toward the gas turbine, where it gets expanded. After expansion in the gas turbine, the exhaust flue gas from the gas turbine is further directed to STC. The STC includes a dual-pressure HRSG,

a high-pressure steam turbine (HPST), a low-pressure steam turbine (LPST), a steam condenser, a deaerator, and feed water pumps. In the HRSG, heat exchange between the gas stream and the water stream is accomplished at two pressure levels. The economizer, evaporator, and superheater are intrinsic components of each pressure level. Steam from the high-pressure section expands in HPST up to lower pressure, and then it is mixed with low-pressure steam to further expand in LPST, as shown in Fig. 1. Wet steam at the outlet of LPST is condensed in the steam condenser. The condensate is then fed to a deaerator with the help of a condensate extraction pump (CEP).

In conjunction with CCGT, a double-effect water–LiBr VARS is employed to cool the compressor inlet air. It consists of an evaporator, absorber, condenser, high-pressure generator (HPG), and low-pressure generator (LPG). Two

solution heat exchangers transfer heat from a hot solution to a cold solution. A compressor’s intake air is cooled by an inlet air cooler. As depicted in Fig. 1, the HRSG exhaust is utilized as a heat input in the HPG vapor absorption system via a heat exchanger.

In this study, the following assumptions are taken into account:

- (i) The kinetic and potential energies of each stream are neglected.
- (ii) Except for the combustion chamber, chemical exergy is neglected.
- (iii) The effectiveness of the condenser, absorber, and evaporator in VARS is assumed to be 100%.
- (iv) The gas leaving the HPG of VARS is maintained at a minimum temperature of 393 K.

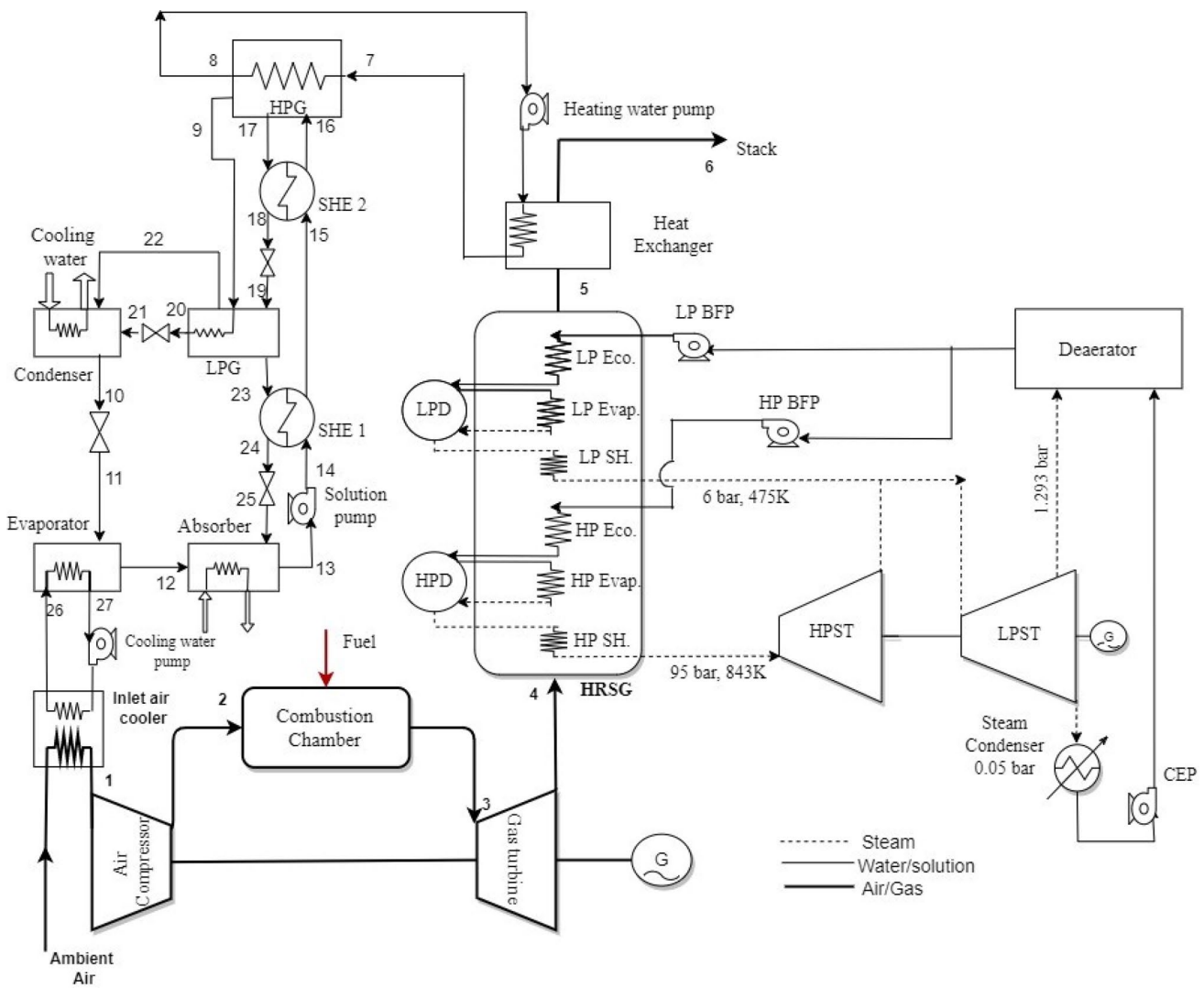


Fig. 1 Schematic diagram of CCGT with double-effect water-LiBr Absorption refrigeration system

2.1 Energy analysis

2.1.1 Air compressor

Air is fed to the compressor at a pressure, P_1 and temperature, T_1 . The exit temperature, T_2 is a function of the polytropic efficiency of the compressor (η_{AC}), pressure ratio (r_p) and specific heat ratio of air (γ_{comp}) as follows:

$$T_2 = T_1 \times \left(1 + \frac{1}{\eta_{AC}} \left(r_p^{\frac{\gamma_{comp}-1}{\gamma_{comp}}} - 1 \right) \right) \tag{1}$$

where η_{AC} is isentropic efficiency of air compressors as given below [22]:

$$\eta_{AC} = 0.91 - \frac{r_p - 1}{300} \tag{2}$$

The required work rate for the compressor is defined as the function of the air mass flow rate (\dot{m}_a), the specific heat ($C_{p,comp}$), temperature difference, and mechanical efficiency of the compressor (η_m).

$$\dot{W}_C = \frac{\dot{m}_a C_{p,comp} (T_2 - T_1)}{\eta_m} \tag{3}$$

Here, $C_{p,comp}$ [41] and γ_{comp} are determined as follows. Hence,

$$C_{pa} = 1.04841 - \left(\frac{3.3871T}{10^4} \right) + \left(\frac{9.4537T^2}{10^7} \right) - \left(\frac{5.49031T^3}{10^{10}} \right) + \left(\frac{7.9298T^4}{10^{14}} \right) \tag{4}$$

$$C_{va} = C_{pa} - 0.287 \tag{5}$$

$$C_{p,vap} = 1.8778 - \left(\frac{5.112T}{10^4} \right) + \left(\frac{1.9157T^2}{10^6} \right) - \left(\frac{1.367T^3}{10^9} \right) + \left(\frac{3.723T^4}{10^{14}} \right) \tag{6}$$

$$C_{v,vap} = C_{p,vap} - 0.4614 \tag{7}$$

$$C_{p,comp} = C_{pa} + \omega_{a,i} C_{p,vap} \tag{8}$$

$$C_{v,comp} = C_{va} + \omega_{a,i} C_{v,vap} \tag{9}$$

$$\gamma_{comp} = \frac{C_{p,comp}}{C_{v,comp}} \tag{10}$$

where $C_{p,vap}$ and $C_{v,vap}$ represent the specific heat of water vapor at constant pressure and constant volume, respectively. $\omega_{a,i}$ represents the specific humidity of air at the compressor's inlet.

2.1.2 Combustion chamber

The flue gas properties from the exit of the combustion chamber are a function of the lower heating value (LHV) of fuel, airflow rate, and efficiency of the combustor (η_{CC}). The following equation exhibits the energy balance in the combustion chamber:

$$\dot{m}_a C_{pa} T_2 + \dot{m}_f \eta_{CC} \cdot LHV = (\dot{m}_a + \dot{m}_f) C_{pg} T_3 \tag{11}$$

The exit pressure is estimated by taking the pressure drop (ΔP_{CC}) into account across the combustion chamber, represented as:

$$P_3 = P_2 (1 - \Delta P_{CC}) \tag{12}$$

Moreover, the properties of combustion products are evaluated via chemical and thermodynamic equilibrium. The chemical reaction of hydrocarbon fuel is considered, according to Ahmadi et al. [1], followed by its chemical equilibrium. Specific heat of combustion products is obtained from the standard theory of mixture by taking the specific heat of all constituents individually for different temperatures [43] as follows:

$$C_{pg} = f_h * [y_1 \cdot C_{p,1} + y_2 \cdot C_{p,2} + y_3 \cdot C_{p,3} \dots \dots y_n \cdot C_{p,n}] \tag{13}$$

where $i = 1, 2, 3, \dots$ represents the constituents and $y_i = \frac{m_i}{m}$ f_h is known as the humidity correction factor [31] and represented as

$$f_h = 1 + 0.05\varphi \tag{14}$$

where φ is relative humidity at the exit of the inlet air cooler.

2.1.3 Gas turbine

Similar to the compressor, the outlet temperature from the gas turbine is a function of the polytropic efficiency of the gas turbine (η_{GT}), pressure ratio ($\frac{P_3}{P_4}$) across the gas turbine, and the specific heat ratio of the gas (γ_g).

$$T_4 = T_3 \times \left(1 - \eta_{GT} \left(1 - \left(\frac{P_3}{P_4} \right)^{\frac{1-\gamma_g}{\gamma_g}} \right) \right) \tag{15}$$

A correlation for isentropic efficiency of the gas turbine as a function of ($\frac{P_3}{P_4}$) can be given as [22]:

$$\eta_{GT} = 0.90 - \frac{\left(\frac{P_3}{P_4}\right) - 1}{250} \tag{16}$$

The expansion work rate from the gas turbine is estimated by considering the flue gas flow rate (\dot{m}_g), gas-specific heat (C_{pg}), the temperature difference between entry and exit, and mechanical efficiency (η_m).

$$\dot{W}_{GT} = \dot{m}_g C_{pg} (T_3 - T_4) \cdot \eta_m \tag{17}$$

2.1.4 Heat recovery steam generator

Each component of the dual pressure HRSG maintains energy balance for the gas and water streams. The equations are listed in Table 1.

2.1.5 Steam turbines

The work generation rate from HPST is obtained by the expansion of steam coming from the high-pressure section of HRSG up to lower pressure. This steam is adiabatically mixed with low-pressure steam coming from the low-pressure section of HRSG. Likewise, the mixed steam is expanded in LPST to produce further work. The energy equations of both steam turbines are as follows:

$$\dot{W}_{HPST} = \eta_m \cdot \eta_{isen, hpst} \cdot \dot{m}_{s, hp} (h_{hp, sh, ex} - h_{lp, sh, ex}) \tag{18}$$

$$\dot{m}_{s, lp} + \dot{m}_{s, hp} = \dot{m}_s \tag{19}$$

Here, \dot{m}_s is the total mass flow rate of steam that is to be expanded in LPST.

$$\dot{W}_{LPST} = \eta_m \cdot \eta_{isen, lpst} \cdot (\dot{m}_s (h_{lp, sh, ex} - h_{lpst, dea, pres}) + (\dot{m}_s - \dot{m}_{s, dea}) (h_{lpst, dea, pres} - h_{lpst, ex})) \tag{20}$$

Table 1 Energy balance equations in HRSG components

HRSG component	Equations
HP superheater	$\dot{m}_g C_{pg} (T_4 - T_{4a}) = \dot{m}_{s, hp} (h_{hp, sh, ex} - h_{hp, sh, in})$
HP evaporator	$\dot{m}_g C_{pg} (T_{4a} - T_{4b}) = \dot{m}_{s, hp} (h_{hp, evap, ex} - h_{hp, evap, in})$
HP economizer	$\dot{m}_g C_{pg} (T_{4b} - T_{4c}) = \dot{m}_{s, hp} (h_{hp, eco, ex} - h_{hp, eco, in})$
LP superheater	$\dot{m}_g C_{pg} (T_{4d} - T_{4e}) = \dot{m}_{s, lp} (h_{lp, sh, ex} - h_{lp, sh, in})$
LP evaporator	$\dot{m}_g C_{pg} (T_{4e} - T_{4f}) = \dot{m}_{s, lp} (h_{lp, evap, ex} - h_{lp, evap, in})$
LP economizer	$\dot{m}_g C_{pg} (T_{4f} - T_5) = \dot{m}_{s, lp} (h_{lp, eco, ex} - h_{lp, eco, in})$

2.1.6 Steam condenser

The exiting steam from LPST is condensed in the steam condenser. The energy balance between the steam and cooling water is depicted as follows:

$$(\dot{m}_s - \dot{m}_{s, dea}) (h_{lpst, ex} - h_{cond, ex}) = \dot{m}_{cw} C_{p, cw} (t_{cw, in} - t_{cw, out}) \tag{21}$$

2.1.7 Deaerator

The deaerator removes dissolved gases such as O₂ and CO₂ from the condensate by using steam bled from the LPST; as a result, feed water is obtained at deaerator pressure. Deaerator pressure is calculated using the deaerator temperature ratio for the optimum heat recovery from the exhaust [23]:

$$\theta_{dea} = \frac{T_{fw, dea, ex} - T_{cond}}{T_{fw, sat, hp} - T_{cond}} \tag{22}$$

The mass flow rate of steam bled for deaeration is calculated with the help of energy balance as follows:

$$\dot{m}_{s, dea} (h_{s, dea, in} - h_{cep, ex}) = \dot{m}_s (h_{fw} - h_{cep, ex}) \tag{23}$$

2.1.8 Condensate extraction pump

The work input rate in CEP is given as:

$$\dot{W}_{cep} = \frac{(\dot{m}_s - \dot{m}_{s, dea}) (h_{cep, ex} - h_{cond, ex})}{\eta_{m, cep}} \tag{24}$$

2.1.9 Boiler feed pumps

The required work input rate for low- and high-pressure boiler feed pumps (BFP), respectively, is written as:

$$\dot{W}_{BFP, lp} = \frac{\dot{m}_{s, lp} (h_{hrsg, lp} - h_{fw})}{\eta_{m, BFP, lp}} \tag{25}$$

$$\dot{W}_{BFP, hp} = \frac{\dot{m}_{s, hp} (h_{hrsg, hp} - h_{fw})}{\eta_{m, BFP, hp}} \tag{26}$$

The total work output of standalone CCGT is given as:

$$\dot{W}_{CCGT} = \dot{W}_{GT} - \dot{W}_C + \dot{W}_{HPST} + \dot{W}_{LPST} - \dot{W}_{BFP, lp} - \dot{W}_{BFP, hp} - \dot{W}_{cep} \tag{27}$$

The efficiency of standalone CCGT is established as

$$\eta_{CCGT} = \frac{\dot{W}_{CCGT}}{\eta_{CC} \cdot \dot{m}_f \cdot LHV} \tag{28}$$

2.1.10 Double-effect water-LiBr VARS

The working fluid for series flow double-effect VARS comprises a refrigerant (Water) and an absorbent (LiBr) [37]. It is modeled using the approach and assumptions of Gomri and Hakimi [17]. The thermodynamic properties (enthalpy and entropy) of water-LiBr solution at different points are calculated using the correlations suggested by Pátek and Klomfar [33].

The concentrations of strong solution (function of the absorber and evaporator temperature) and weak solution (function of VARS condenser and LPG temperature) are calculated as follows [25]:

$$X_{ss} = \frac{49.04 + 1.125t_a - t_e}{134.65 + 0.47t_a} \quad (29)$$

$$X_{ws} = \frac{49.04 + 1.125t_{LPG} - t_c}{134.65 + 0.47t_{LPG}} \quad (30)$$

The concentration of the medium solution (X_{ms}) lies between X_{ws} and X_{ss} . X_{ms} is calculated using an iterative method unless the energy balance in LPG reaches up to 10^{-4} kW [17]. Hence, the mass flow rate of weak, strong, and medium solutions is calculated using the concentration values. The energy balance in LPG is given as follows:

$$Q_{LPG} = m_9h_9 + m_{19}h_{19} = m_{20}h_{20} + m_{22}h_{22} + m_{23}h_{23} \quad (31)$$

The concentration value should be less than the critical concentration to eliminate crystallization at any point in the system. The critical concentration as a function of temperature (in °C) was developed by a dynamic simulation model for double-effect VARS [15]. It can be expressed as:

$$X_C = 0.0809 \times t + 61.341 \quad (32)$$

The heat load in HPG and evaporator is given by:

$$Q_{HPG} = m_{g,HPG} C_{pg} (T_5 - T_6) = m_9h_9 + m_{17}h_{17} - m_{16}h_{16} \quad (33)$$

$$Q_{evap} = m_{a,evap} C_{pa} (T_0 - T_1) = m_{12}h_{12} - m_{11}h_{11} \quad (34)$$

The energy balance in the condenser and absorber is written as follows:

$$Q_{cond} = m_{w,cond} C_{pw} (\Delta T_{w,cond}) = m_{21}h_{21} + m_{22}h_{22} - m_{10}h_{10} \quad (35)$$

$$Q_{abs} = m_{w,abs} C_{pw} (\Delta T_{w,abs}) = m_{12}h_{12} + m_{25}h_{25} - m_{13}h_{13} \quad (36)$$

The overall performance of VARS is estimated by evaluating its COP, represented as:

$$COP = \frac{Q_{evap}}{Q_{HPG} + \dot{W}_{SP}} \quad (37)$$

where \dot{W}_{SP} is work input rate to the solution pump and expressed as:

$$\dot{W}_{SP} = m_{13} \frac{(P_{HPG} - P_{abs.})}{n_{sp} \rho_{13}} \quad (38)$$

Now, the total work output of an inlet air cooling integrated system (i.e., CCGTV) is calculated as

$$\dot{W}_{CCGTV} = \dot{W}_{CCGT} - \dot{W}_{SP} \quad (39)$$

$$\eta_{CCGTV} = \frac{\dot{W}_{CCGTV}}{\eta_{CC} \dot{m}_f LHV} \quad (40)$$

2.2 Exergy analysis

Exergy analysis is the thermodynamic analysis that rationally evaluates a system using the first and second laws of thermodynamics. It enables the evaluation and comparison of processes and scope for improvement by eliminating component-wise irreversibility [1]. In a control volume, the exergy balance is written as:

$$\frac{dE_{CV}}{dt_j} = \Sigma \left(1 - \frac{T_0}{T_i} \right) \dot{Q}_i - \left(\dot{W} - P_0 \frac{dV_{CV}}{dt} \right) + \sum_i \dot{m}_i e_i - \sum_e \dot{m}_e e_e - \dot{E}x_D \quad (41)$$

If the rate of energy exchange across the control volume is zero, the equation will be obtained as [21]:

$$\dot{E}x_Q + \sum_i \dot{m}_i e_i = \sum_e \dot{m}_e e_e + \dot{E}x_W + \dot{E}x_D \quad (42)$$

where e is exergy and $\dot{E}x_D$ is exergy destruction rate in kW.

$$\dot{E}x_D = T_0 \dot{S}_{gen} \quad (43)$$

$$\dot{E}x_Q = \left(1 - \frac{T_0}{T_i} \right) \dot{Q}_i \quad (44)$$

$$\dot{E}x_W = \dot{W} - P_0 \frac{dV_{CV}}{dt} \quad (45)$$

$$e_{ph} = (h - h_0) - T_0 (s - s_0) \quad (46)$$

2.2.1 Plant fuel exergy

The exergy assessment of combustion is calculated by considering the physical exergies of flowing streams and the chemical exergy of fuel [14]. The total exergy component of fluid is written as:

$$\dot{E}x_{total} = \dot{E}x_{ph} + \dot{E}x_{ch} \tag{47}$$

The physical exergy of fuel is calculated using the ideal model of gas [32].

$$\dot{E}x_{ph} = \dot{m}_f C_p^h (T - T_0) - \dot{m}_f T_0 \left[C_p^s \ln \frac{T}{T_0} - R \ln \frac{P}{P_0} \right] \tag{48}$$

The mean specific heat for calculating enthalpy and entropy is depicted as:

$$C_p^h = \frac{1}{T - T_0} \int_{T_0}^T C_p dT \tag{49}$$

$$C_p^s = \frac{1}{\ln \frac{T}{T_0}} \int_{T_0}^T C_p dT \tag{50}$$

The chemical exergy fuel (ex_f^{ch}) is calculated using the following relation [3]:

$$\xi = \frac{ex_f^{ch}}{LHV} \tag{51}$$

the value of ξ is close to unity for common gaseous fuels [9]. The value ξ is taken as 1.06 for methane.

An experimental correlation is useful to calculate the value of ξ for any gaseous fuel with a composition $C_x H_y$ [14]:

$$\xi = 1.033 + 0.0169 \frac{y}{x} - \frac{0.0698}{x} \tag{52}$$

The expressions for exergy destruction rate and energetic efficiency for each component of CCGT are represented in Table 2.

2.3 Exergy-based sustainability indicators

Exergy analysis is an attractive method to assess the sustainability level of several energy systems. Sustainability is described as a policy of supplying energy resources at a reasonable cost and with little or no environmental impact [28]. Several sustainability indicators have been examined for the CCGT system based on the theoretical foundation for exergy analysis. Moreover, the effect of inlet air cooling on these parameters has been discussed.

The following exergy-based sustainability indicators [40] considered for this study are:

- (i) Fuel depletion ratio
- (ii) Exergetic improvement potential
- (iii) Environmental effect factor
- (iv) Environmental sustainability index

2.3.1 Fuel depletion ratio

The fuel depletion ratio is the ratio of the exergy destruction rate in a component to the fuel exergy. A lower fuel depletion ratio is preferred because it indicates that the system has

Table 2 Equations for exergy destruction rate and exergetic efficiency for various components

Component	Exergy destruction rate	Exergetic efficiency
Air compressor	$\dot{E}x_{D,AC} = \dot{E}x_1 - \dot{E}x_2 + \dot{W}_{AC}$	$\eta_{ex,AC} = \frac{\dot{E}x_2 - \dot{E}x_1}{\dot{W}_{AC}}$
Combustion chamber	$\dot{E}x_{D,CC} = \dot{E}x_2 - \dot{E}x_3 + \dot{E}x_f$	$\eta_{ex,CC} = \frac{\dot{E}x_3}{\dot{E}x_2 + \dot{E}x_f}$
Gas turbine	$\dot{E}x_{D,GT} = \dot{E}x_3 - \dot{E}x_4 - \dot{W}_{GT}$	$\eta_{ex,GT} = \frac{\dot{W}_{GT}}{\dot{E}x_3 - \dot{E}x_4}$
HRSG	$\dot{E}x_{D,HRSG} = \sum_{i,HRSG} \dot{E}x - \sum_{o,HRSG} \dot{E}x$	$\eta_{ex,HRSG} = \frac{\sum_{i,water} \dot{E}x - \sum_{i,steam} \dot{E}x}{\dot{E}x_4 - \dot{E}x_5}$
HPST	$\dot{E}x_{D,HPST} = \dot{E}x_{i,HPST} - \dot{E}x_{o,HPST} - \dot{W}_{HPST}$	$\eta_{ex,HPST} = \frac{\dot{W}_{HPST}}{\dot{E}x_{i,HPST} - \dot{E}x_{o,HPST}}$
LPST	$\dot{E}x_{D,LPST} = \dot{E}x_{i,LPST} - \dot{E}x_{o,LPST} - \dot{W}_{LPST}$	$\eta_{ex,LPST} = \frac{\dot{W}_{LPST}}{\dot{E}x_{i,LPST} - \dot{E}x_{o,LPST}}$
Condenser	$\dot{E}x_{D,Cond} = \sum_{i,Cond} \dot{E}x - \sum_{o,Cond} \dot{E}x$	$\eta_{ex,Cond} = 1 - \frac{\dot{E}x_{D,Cond}}{\sum_{i,Cond} \dot{E}x}$
Boiler feed pump	$\dot{E}x_{D,BFP} = \dot{E}x_{i,BFP} - \dot{E}x_{o,BFP} + \dot{W}_{BFP}$	$\eta_{ex,BFP} = \frac{\dot{E}x_{o,p} - \dot{E}x_{i,p}}{\dot{W}_{BFP}}$

destroyed less exergy corresponding to fuel exergy. Consequently, more exergy is available at the output [40].

$$\text{Fuel depletion ratio} = \frac{\dot{E}x_{D,\text{component}}}{\dot{E}x_{\text{fuel}}} \quad (53)$$

2.3.2 Environmental effect factor

Environmental effect factor (r_{eef}) is a crucial sustainability factor that is defined as the ratio between waste exergy ratio (WER) and exergetic efficiency. It specifies the severity of environmental damage because of exergy destruction. As a result, r_{eef} is preferred to have low value.

$$\text{WER} = \frac{\text{Total exergy waste}}{\text{Total exergy input}} \quad (54)$$

$$r_{\text{eef}} = \frac{\text{WER}}{\eta_{\text{ex}}} \quad (55)$$

2.3.3 Environmental sustainability index

It is another vital parameter to assess the sustainability level of the system. As a definition, it is represented by the reciprocal of r_{eef} . This index has a value between 0 and 1. A higher exergetic efficiency indicates less waste exergy and a lesser environmental impact, resulting in an increased environmental sustainability index (ESI) of the system. Therefore, an ESI close to 1 indicates a more environmentally sustainable system [39].

$$\text{ESI} = \frac{1}{r_{\text{eef}}} \quad (56)$$

2.3.4 Exergetic improvement potential rate

The exergetic improvement potential is associated with the combined effect of exergetic efficiency and the exergy destruction rate. A higher improvement potential advocates that the system requires improvement over time [40]. Hence, a low exergetic improvement potential is preferred.

$$\text{Exergetic improvement potential rate} = (1 - \eta_{\text{ex}}) \times \dot{E}x_D \quad (57)$$

Figure 2 presents a flowchart that outlines the sequential steps of the thermodynamic simulation process in a logical manner. The flowchart ultimately leads to a comparison of performance parameters and sustainability indicators

under different situations, specifically with and without inlet air cooling.

3 Model validation

Validation of the numerical model established for this system is a necessary step to remove ambiguities and build confidence in the accuracy of the results. The results of this study are validated with previously published papers on related topics. The model of water-LiBr double-effect VARS has been validated by an experimental study of the micro-scale absorption chiller by Yin et al. [45]. The input parameters of Yin et al. [45] are used for generating results from the program made in MATLAB. Table 3 shows the comparison of results obtained from the present model and experimental results of Yin et al. [45] for validation. The simulated results exhibit a maximum deviation of 5.34% from the experimental data. Moreover, the gas cycle-specific work and thermal efficiency of the present study are compared with those substantiated by Mohapatra and Sanjay [29] at ambient conditions of 303 K and RH = 20%, as shown in Fig. 3. Both parameters are in good agreement with each other, within 4% of the variation. The COP of the water-LiBr vapor absorption system decreases with an increase in ambient temperature, as compared to the trend with Ren et al. [36]. The variation of r_{eef} and ESI against the exergetic efficiency of the system shows a similar trend to those reported by Eke et al. [11].

4 Results and discussion

The performance of the standalone CCGT system along with its integration with a double-effect vapor absorption system is investigated with realistic input data. The input parameters for the analysis are presented in Table 4. Utilizing governing equations, a MATLAB program was developed for the analysis, and input data were used to obtain the results.

4.1 Effect of ambient temperature and IAC on energy parameters

Based on the thermodynamic equations mentioned in Sect. 2.1, energy analysis is the primary criterion for the assessment of the CCGT and CCGTV. Energy performance encapsulates the total work output and thermal efficiency as the key performance parameters for the comparison of both cases.

The plant-specific work output as a function of ambient temperature is depicted in Fig. 4. The compressor's inlet temperature rises as the ambient temperature rises, resulting

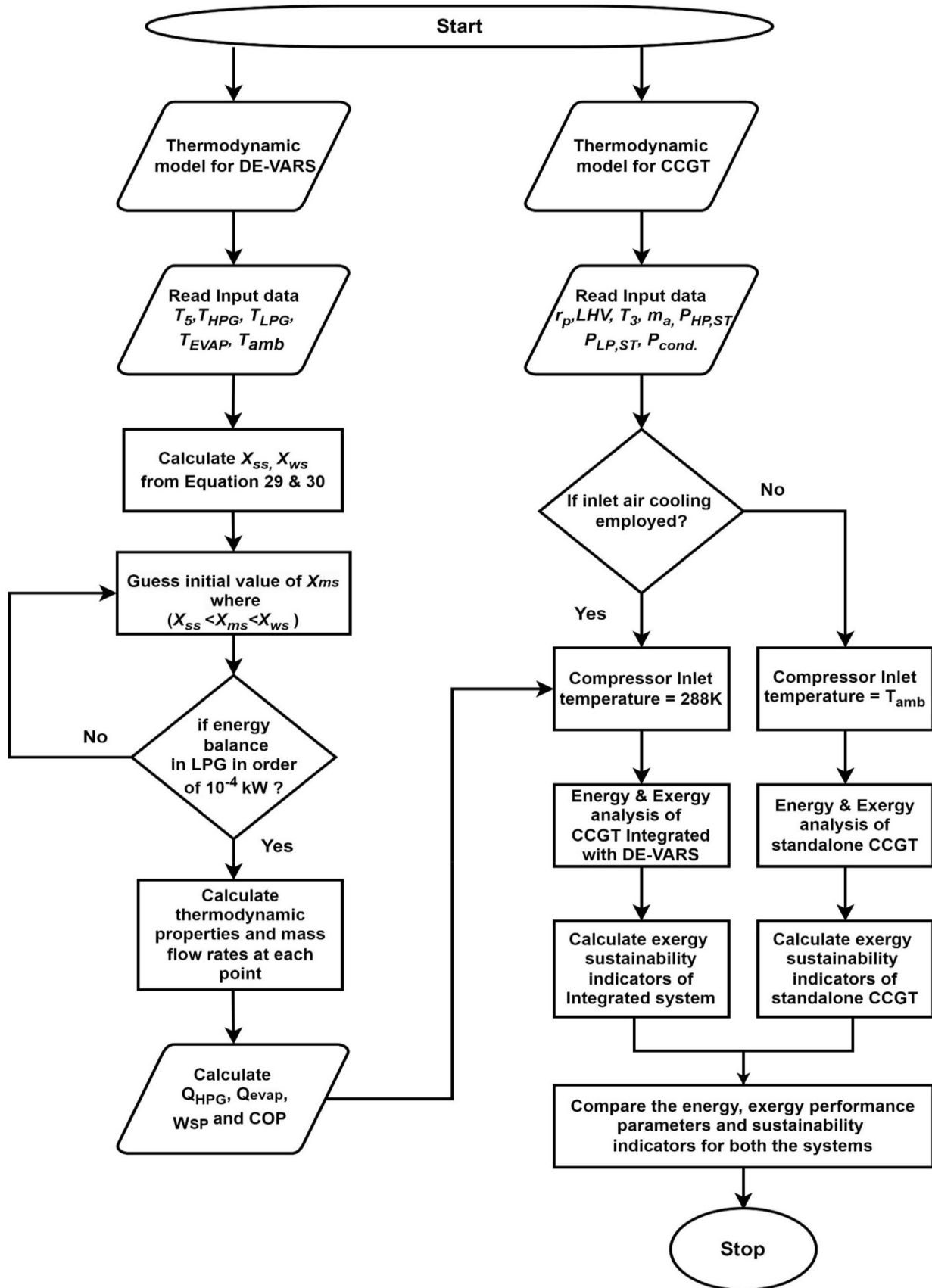
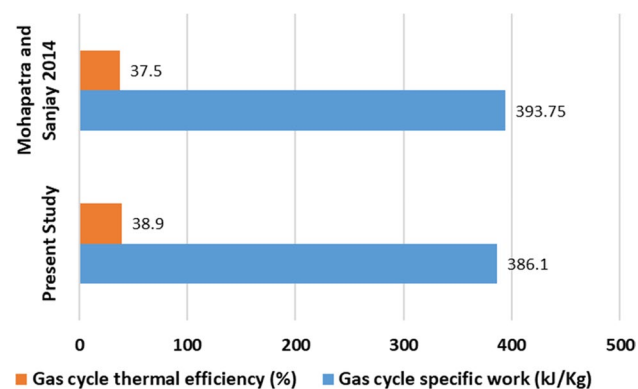


Fig. 2 A mathematical framework and flow-chart of the thermodynamic simulation process

Table 3 Model validation of Water-LiBr double-effect VARS

Input parameters		Value	
Chilled water inlet temperature		13.9 °C	
Cooling water temperature		30.78 °C	
Cooling water mass flow rate		1.546 kg/s	
Chilled water mass flow rate		0.5616 kg/s	
Output value	Simulation results	Experimental results [45]	Difference between simulation and experimental results (%)
Chilled water outlet temperature	7.05 °C	7 °C	0.71
Cooling effect	17.19 kW	16.63 kW	3.36
COP	1.0851	1.03	5.34

in more compression work. As a result, the specific work output rate in CCGT decreases. When the compressor inlet temperature (CIT) is fixed at 288 K via inlet air cooling, the CCGTV specific work increases by 2.07 to 5.04% when the ambient temperature rises from 290 to 306 K. On the contrary, CCGTV-specific work decreases across the range because, in order to keep CIT at 288 K, VARS must fetch more heat from the HRSG as the ambient temperature rises. As shown in Fig. 4, increased temperature exhaust is required at the HRSG exit. It eventually leads to less STC-specific work. The COP of VARS as a function of ambient temperature is also shown in Fig. 5. When the ambient temperature rises from 290 to 306 K, the COP falls to 0.83 from 1.44. The reason for this is that as the ambient temperature rises, the evaporator must absorb more heat from the surrounding air in order to maintain CIT at 288 K. To increase the heat intake from the evaporator, the VARS must generate more refrigerant, which ultimately increases the heat supplied by the HRSG exhaust at the HPG. However, as the ambient temperature rises, the heat input in HPG rises faster than the heat intake in the evaporator, resulting in a decrease in the COP of VARS.

**Fig. 3** Comparison of gas cycle specific work and efficiency results from the present study with Mohapatra and Sanjay [29]

Similarly, in Fig. 6, the thermal efficiency is shown as a function of ambient temperature. The thermal efficiency of CCGTV is found to be higher than CCGT, which also indicates lesser fuel consumption per unit of work output. At 290 K, an improvement of 1.58% is observed, which increases to 1.64% at 296 K and then decreases to 1.23% at 306 K. Thus, when the temperature difference between cooled air and ambient air (i.e., the degree of cooling) is 8K, the greatest increase in thermal efficiency is observed.

4.2 Effect of ambient temperature and IAC on exergetic performance

The exergetic performance summarizes the exergy destruction rate and exergetic efficiency of each component and the complete system. Figure 7 depicts the exergetic efficiency of the system as a function of ambient temperature. As the ambient temperature rises, the exergetic efficiency decreases. Since the high CIT decreases the useful exergy (net work output) in CCGT, the resulting exergetic efficiency decreases. After maintaining the CIT at 288 K with the help of inlet air cooling, exergetic efficiency is found to be improved. CCGTV is 1.23 to 1.64% more exergetically efficient than CCGT over the specified ambient temperature range. However, the specific exergy destruction in CCGTV is 0.91% lower than in CCGT at 290 K, and the same becomes 1.46% higher at 306 K. This increase is due to an increased fuel supply in the combustion chamber and the addition of the VARS to the existing CCGT. Table 5 shows the component-wise specific exergy destruction in each component. Among all components, the combustion chamber is shown to be the largest exergy destroyer. In both cases, the contribution of the exergy destruction in the combustion chamber is greater than 60.32% of the total specific exergy destruction. These outcomes are owing to the enormous irreversibilities associated with

Table 4 Input data for the simulation [16, 31, 37]

Component	Parameter	Unit
Compressor	Compression ratio (P_r) = 20–24	–
	Mechanical efficiency ($\eta_{m,comp}$) = 98.5%	–
Combustion chamber	Combustion efficiency (η_{cc}) = 99.5%	–
	LHV of fuel = 47,200	kJ/kg
	Fuel composition CH ₄ = 100%	–
	Air composition (by volume) = 21% O ₂ , 79% N ₂	–
	Pressure drop = 3% of entry pressure	–
Gas turbine	Turbine inlet temperature (T_3) = 1500–1750	K
	Flue gas exhaust pressure = 1.093	bar
	Mechanical efficiency ($\eta_{m,GT}$) = 98.5%	–
HRSG	HP steam pressure = 95	bar
	LP steam pressure = 5	bar
	HP steam temperature = 843	K
	LP steam temperature = 475	K
Stack	Stack exhaust temperature \geq 393	K
Steam turbine	Mechanical efficiency ($\eta_{m,ST}$) = 98.5%	–
	Isentropic efficiency ($\eta_{isen,LPST}$) = 92%	–
	Isentropic efficiency ($\eta_{isen,HPST}$) = 88%	–
	Steam quality at LPST exit = 0.88	–
Steam condenser	Condenser pressure = 0.05	bar
Deaerator	Deaerator pressure = 1.293	bar
	Deaerator temperature ratio = 0.27	–
BFP	Efficiencies of Boiler feed pumps = 80%	–
CEP	Condensate extraction pump pressure = 1.293	bar
VARs	Effectiveness of HPG = 0.96	–
	Evaporator temperature (T_{evap}) = 278	K
	HRSG exhaust temperature \leq 423	K
	SHE effectiveness = 70%	–
	Mechanical efficiency of the solution pump ($\eta_{m,SP}$) = 95%	–

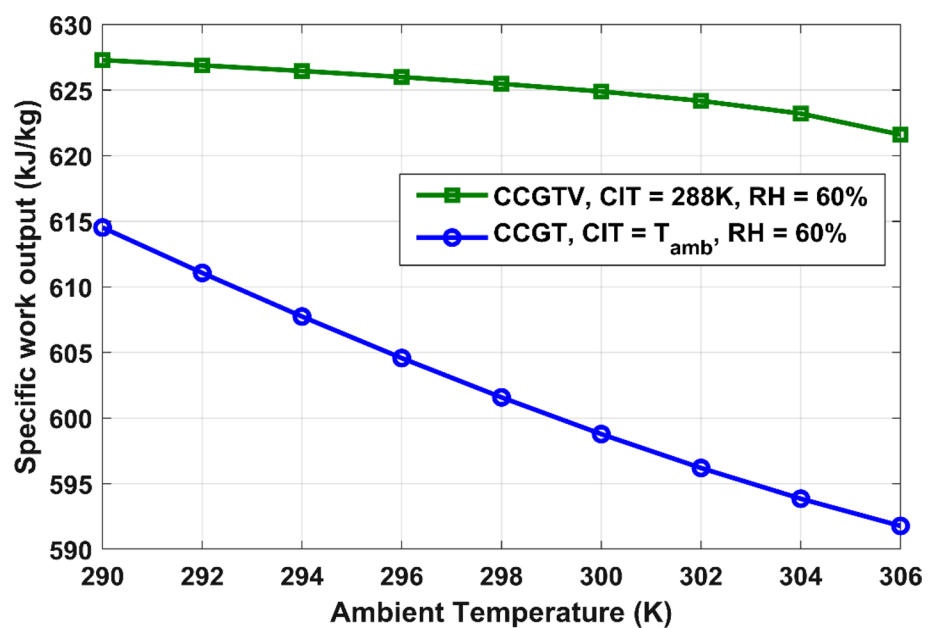
Fig. 4 Effect of ambient temperature on specific work output

Fig. 5 Effect of ambient temperature on the COP of VARS and HRSG exhaust temperature

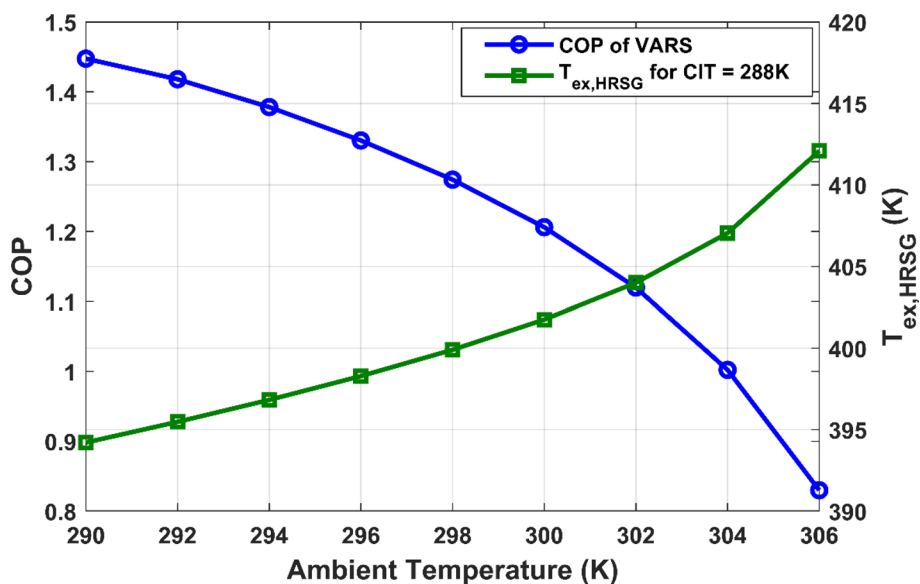
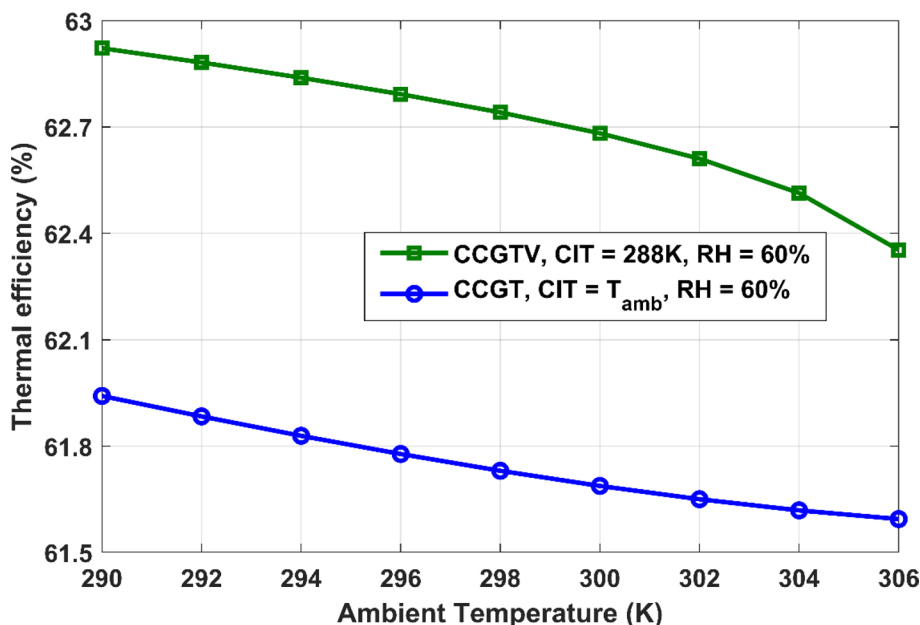


Fig. 6 Effect of ambient temperature on the overall thermal efficiency



chemical reactions and heat transfer across substantial temperature differences between compressed air and fuel.

4.3 Effect of other influential parameters on the performance

In addition to ambient temperature, the thermodynamic performance of CCGT and CCGTV, as well as the effect of other influential parameters including gas turbine inlet temperature (TIT) and pressure ratios, has been investigated. Figure 8 depicts the variations in specific work output and exergetic efficiency of CCGT and CCGTV. The specific work output and exergetic efficiency both decrease

as the ambient temperature rises, which is also validated by previous results. However, increasing the pressure ratio from 20 to 23 marginally reduces the total work output. The reason being as the compressor work increases, the net work production decreases. Also, as a result of the increased pressure ratio, the temperature of compressor exhaust air rises, and the fuel intake would decrease to achieve a TIT of 1750 K. The effect of inlet air cooling has also been shown in the results. Additionally, the reduction in TIT from 1750 to 1600 K has a considerable impact on both performance factors. The decline in gas turbine work production and fuel supply is attributed to the fact that the former diminishes at faster rates than the latter. Along with

Fig. 7 Effect of ambient temperature on exergetic efficiency

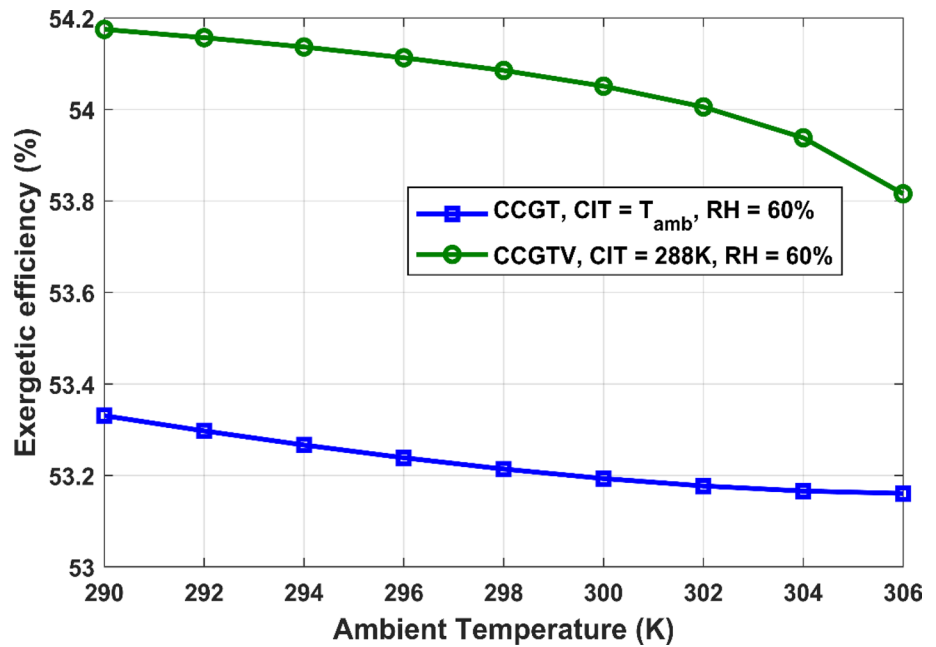
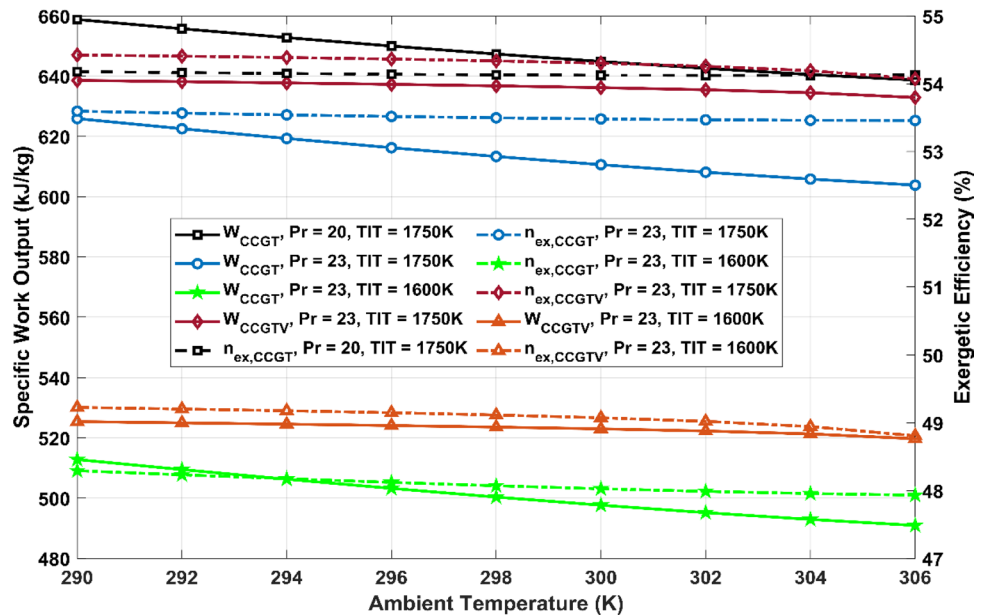


Fig. 8 Effect of TIT, pressure ratio, and inlet air cooling on the specific work output and exergetic efficiency



that, it is noteworthy that for the same pressure ratio, TIT, and the same increase in ambient temperature, the rate of change (i.e., decrease) in both parameters, whether CCGT or CCGTV, is nearly identical.

As a result of inlet air cooling, it is necessary to analyze the variation in several performance factors. This analysis may suggest points in the working range at which multiple parameters are favorable. As the ambient temperature ranges from 290 to 306 K, it is intriguing to learn how each operating and performance parameter increases or decreases when CCGT is replaced by CCGTV with a CIT of 288 K.

Figure 9 depicts the percentage change in those parameters over the degree of cooling ranges from 2 to 18 K. The rate of fuel intake into the combustion chamber increases as the air cools before the compressor. With it, the rate of increment of total work also increases. Since total work consists of GTC and STC-specific works, as the degree of cooling increases, the increase in gas turbine work increases, while the increase in steam turbine work decreases. The increase in gas turbine efficiency is correlated with the constant reduction of compressor work caused by cooled air. The increase in STC-specific work is a result of the increased flue gas rate in the GTC, followed by the HRSG as a result of cooling.

Fig. 9 Effect of degree of cooling on variation in several parameters of CCGTV

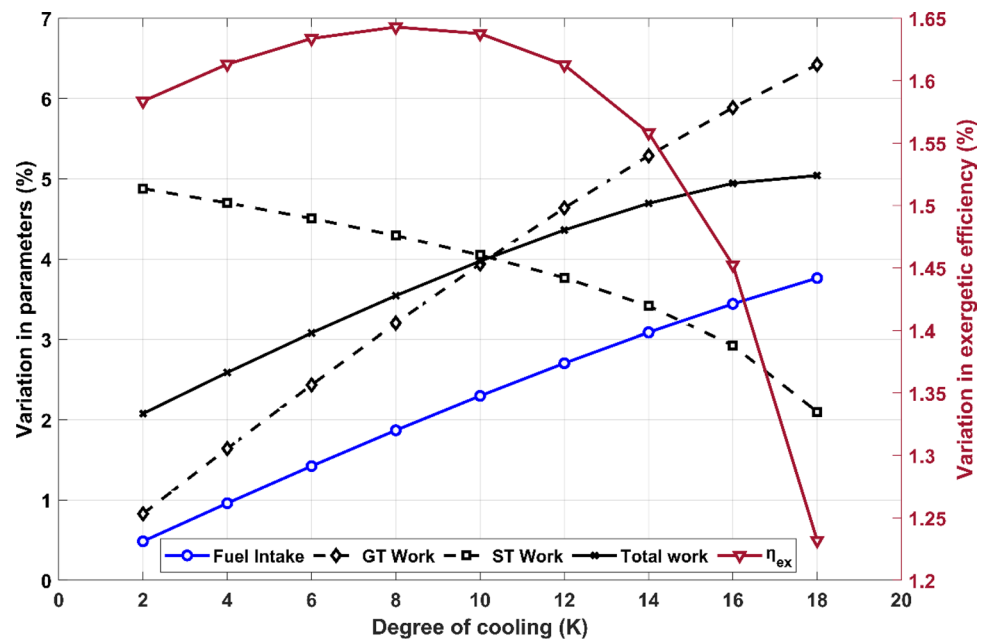


Table 5 Specific exergy destruction in various components

Component	Specific exergy destruction (kJ/kg)	
	CCGT	CCGTV
Compressor	36.45–44.70	44.94–45.93
Combustion chamber	476.55–502.38	478.31–507.94
Gas turbine	58.52–61.40	58.46–60.89
HRSG	106.17–111.58	102.51–110.57
HPST	20.28–20.70	21.13–21.27
LPST	34.81–36.01	36.51–36.76
Steam condenser	20.35–47.27	21.08–50.32
VARS	–	2.14–2.45
Stack	17.33–23.77	13.13–14.41

However, as the degree of cooling increases, STC-specific work decreases because VARS requires more energy from HRSG exhaust, thereby reducing the steam production rate. And as the cooling approaches a higher degree, the effect of decreasing increment in STC-specific work becomes predominant. As a result, the rate of increase in total work has been observed to decrease as the degree of cooling increases. After 18 K of inlet air cooling, the total work curve could begin to flatten or decrease. In contrast, the increase in the exergetic efficiency of the entire system continues up until 8 K of air inlet cooling. After that, it decreases until the degree of cooling reaches 18 K.

This result suggests that the optimal degree of cooling for CCGTV, in terms of total work output and exergetic efficiency, is between 8 and 18 K. CCGTV can operate with a cooling degree of 18 K to generate maximum work and

with a cooling degree of 8 K to maximize yield in exergetic efficiency. If the price per unit of electricity is high, it may be economically advantageous to operate the CCGTV with 18 K of cooling; if the price per unit of fuel increases, the degree of cooling could approach 8 K in order to balance overall operational costs.

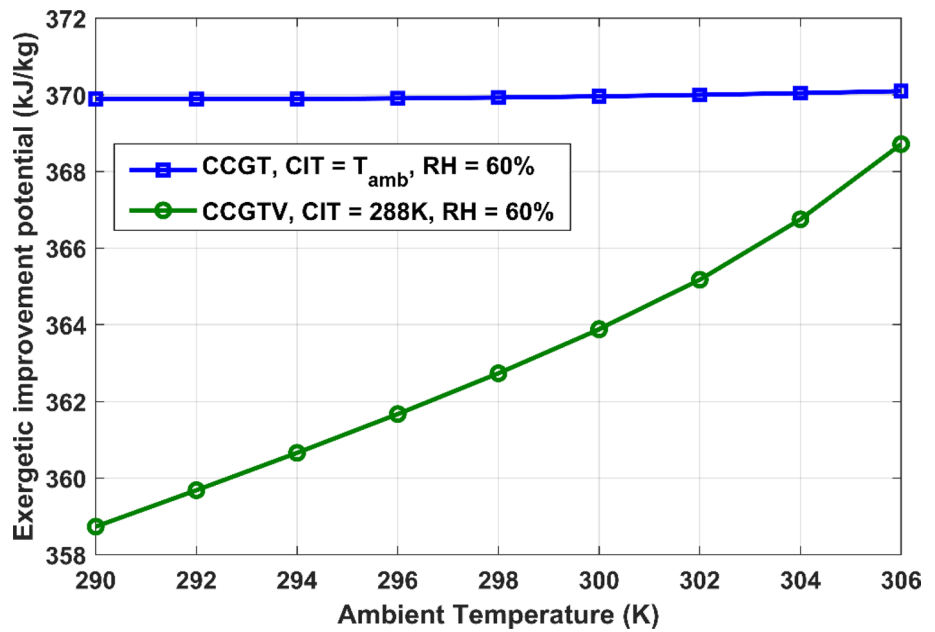
4.4 Effect of IAC on exergy sustainability indicators

The range of fuel depletion ratios for all major components with and without inlet air cooling is shown in Table 6. The total fuel depletion ratio is shown to be 1.38 to 1.26% lower after using inlet air cooling. It suggests that CCGTV with inlet air cooling (i.e., CCGTV) ends up destroying less exergy per unit of fuel than standalone CCGT. Therefore, CCGTV turns out to be more exergetically superior to standalone CCGT. The fuel depletion ratio in both the major exergy

Table 6 Comparison of fuel depletion ratios

Component	Fuel depletion ratio*100 (%)	
	CCGT	CCGTV
Compressor	3.27–3.87	3.88–4.06
Combustion Chamber	41.35–45.12	41.30–43.92
Gas turbine	5.07–5.51	5.04–5.27
HRSG	9.21–10.02	8.85–9.57
HPST	1.76–1.85	1.82–1.83
LPST	3.02–3.23	3.15–3.18
Steam condenser	1.82–4.11	1.82–4.29
Total	68.85–70.74	67.60–69.22

Fig. 10 Effect of ambient temperature on exergetic improvement potential



destroyers, i.e., the combustion chamber and HRSG, is found to be decreased in CCGTV. Figure 10 shows the exergetic improvement potential as a function of ambient temperature. CCGTV has shown lower overall exergetic improvement potential than CCGT. However, the increase in improvement potential in CCGTV is rapid with the increase in ambient temperature. At 290 K, the difference in exergetic improvement potential is 3.07%, which decreases to 0.37% at 306 K. The combustion chamber in CCGTV is found to have marginally increased improvement potential by 0.60 to 1.70%, while HRSG has shown a decline of 2.89 to 8.97% in the same.

Figure 11 demonstrates the effect of increased ambient temperature on the environmental effect factor (r_{eef}) and environmental sustainability index (ESI). The r_{eef} varies between 1.285 and 1.331 for CCGT while for CCGTV, it varies between 1.247 and 1.285, showing a reduction of 2.92 to 3.40% over the specified range. On the other hand, ESI varies from 0.777 to 0.751 for CCGT, and 0.803 to 0.778 for CCGTV, showing an improvement of 3.01–3.52%. Thus, a reduction in r_{eef} shows less damage to the environment after cooling the inlet air. Also, the increase in ESI implies that there is a reduction in waste exergy, as decreasing the CIT is an effective way. Figure 12 shows the variation of r_{eef}

Fig. 11 Effect of ambient temperature on Environmental effect factor and ESI

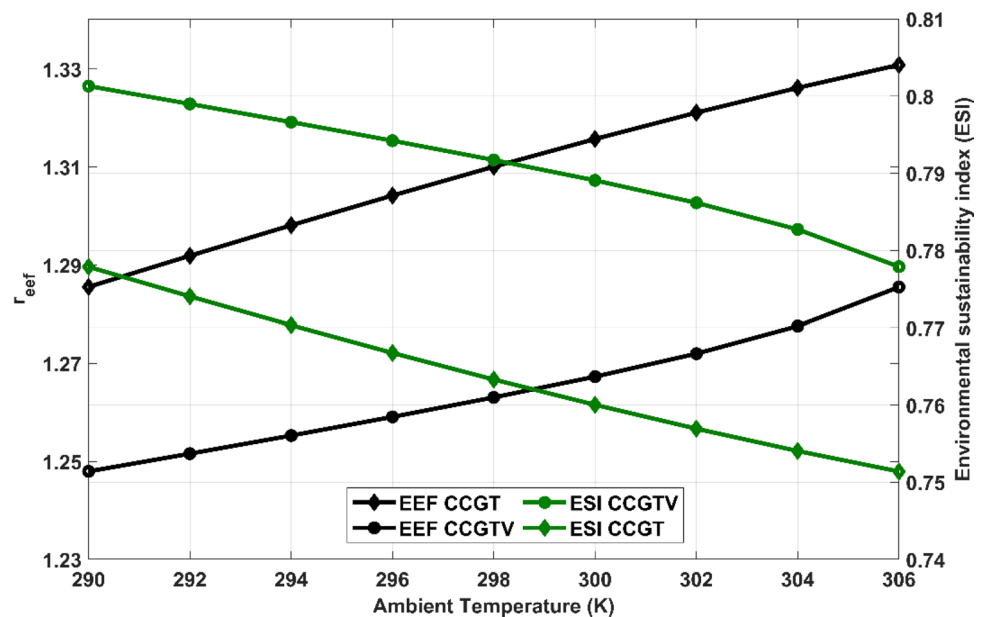


Fig. 12 Variation of exergetic efficiency with Environmental effect factor

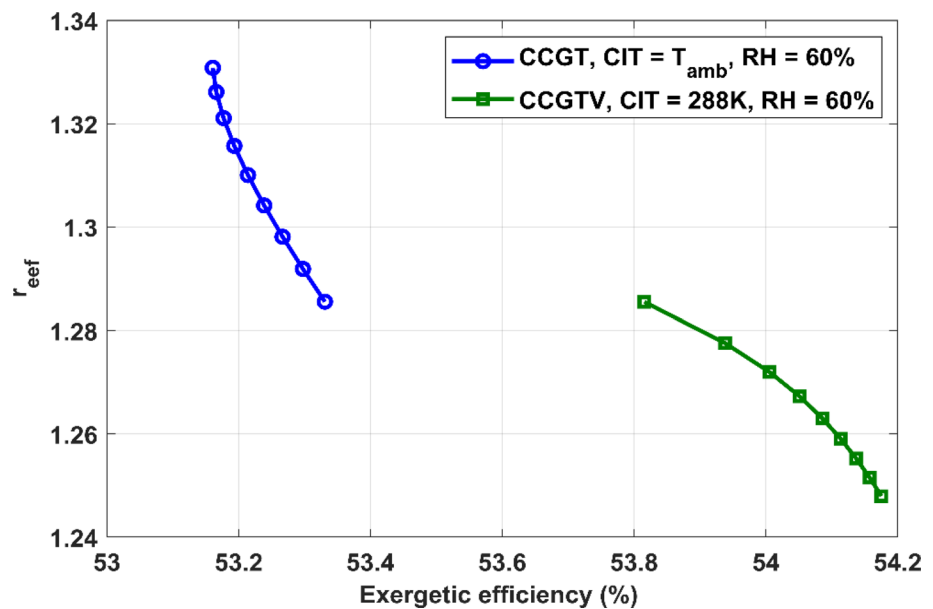


Table 7 Improvement in performance by inlet air cooling in the present analysis as compared to the same in Singh [38]

Performance parameters	Singh [38] (%)	Present analysis (%)
Increase in work output	2.8	5.04
Increase in thermal efficiency	1.193	1.64
Increase in energetic efficiency	1.133	1.64

with exergetic efficiency. As exergetic efficiency increases, the r_{eeef} decreases. Also, the range of r_{eeef} shifted even lower after the integration of inlet air cooling. It implies that the CCGTV is more exergetically efficient because it releases fewer emissions into the atmosphere. Since ESI is reciprocal to r_{eeef} , ESI increases with an increase in exergetic efficiency. Therefore, CCGTV has witnessed greater sustainability due to reduced irreversible losses and, hence, efficient utilization of resources.

5 Conclusion

The CCGT plant has undergone an analysis involving the implementation of inlet air cooling. This process is achieved through the integration of a water-LiBr-based double-effect VARS. The analysis of the system has been conducted using energy, exergy, and exergy-based sustainability indicators. The conclusions that can be inferred from this study are summarized as follows:

- (1) The integration of a double-effect vapor absorption refrigeration system with the CCGT enables an increase in specific work output and thermal efficiency by a maximum of 5.04 and 1.64%, respectively. Table 7 compares the performance improvement of the current system to that of the single-effect Ammonia-water-based VARS inlet air cooling investigated by Singh [38].
- (2) To keep CIT at 288 K, the VARS absorbs more heat from the HRSG's exit, as the COP of the VARS reduces with the rise in ambient temperature. Consequently, a reduction in the steam generation rate has been observed in the bottoming cycle.
- (3) The combustion chamber is the dominant contributor to irreversibility, accounting for $\geq 60.32\%$ of total irreversibility. The CCGT system with inlet air cooling is 1.23–1.64% more exergetically efficient than a standalone CCGT plant.
- (4) After using inlet air cooling, the fuel depletion ratio and exergetic improvement potential are found to be reduced by a maximum of 1.38% and 3.07%, respectively.
- (5) The environmental effect factor for VARS-integrated CCGT has been observed to decrease by 2.92 to 3.40%. Thus, the environmental sustainability index is found to be enhanced.
- (6) In order to maximize the exergetic efficiency and total work output of CCGTV, the suitable degree of inlet air cooling ranges from 8 to 18 K.
- (7) Improved exergetic efficiency reduces the adverse environmental effect and promotes the system's sustainability as a result of efficient utilization of fuel.

Furthermore, effective fuel utilization would help reduce emissions per unit of power generation. This would reduce the cost of post-combustion carbon capture, ultimately accelerating the achievement of decarbonization goals.

The current work can be viewed as an initial effort toward adopting a thermodynamic approach to analyze the reliability of absorption-based inlet air cooling for CCGT power plants. Additionally, it is suggested that future research in this topic should explore the economic aspect using the exergy costing method. This approach should be combined with a multi-objective optimization framework that aims to maximize exergetic efficiency while simultaneously minimizing overall cost. However, based on the study's findings, several technical recommendations (also from the industrial and research and development perspectives) can be made. These recommendations are listed below:

- (1) To enhance the performance of a CCGT plant, warm ambient air should be cooled to the ISO temperature for gas turbines.
- (2) Utilize a waste heat-powered double-effect absorption refrigeration system instead of a mechanical refrigeration system and single effect absorption systems to cool the warm ambient air.
- (3) Put emphasis on minimizing exergy destruction in the combustion chamber as it is the largest exergy destroyer.
- (4) For the intended enhancement of power output and exergetic efficiency, the recommended ambient temperature range for operating the presented system is between 296 and 306 K.

Declarations

Conflict of interest The authors declare no potential conflict of interest with respect to the research, authorship, and publication of this article.

References

1. Ahmadi P, Dincer I, Rosen MA (2011) Exergy, exergoeconomic and environmental analyses and evolutionary algorithm based multi-objective optimization of combined cycle power plants. *Energy* 36(10):5886–5898. <https://doi.org/10.1016/j.energy.2011.08.034>
2. Ahmadzadehtalatapeh M, Rashidi HR (2020) Performance enhancement of gas turbine units by retrofitting with inlet air cooling technologies (IACs): an hour-by-hour simulation study. *J Braz Soc Mech Sci Eng* 42(3):139. <https://doi.org/10.1007/s40430-020-2216-7>
3. Ameri M, Mokhtari H, Mostafavi Sani M (2018) 4E analyses and multi-objective optimization of different fuels application for a large combined cycle power plant. *Energy* 156:371–386. <https://doi.org/10.1016/j.energy.2018.05.039>
4. Baakeem SS, Orfi J, Al-Ansary H (2018) Performance improvement of gas turbine power plants by utilizing turbine inlet air-cooling (TIAC) technologies in Riyadh, Saudi Arabia. *Appl Therm Eng* 138:417–432. <https://doi.org/10.1016/j.applthermaleng.2018.04.018>
5. Boyce MP (2012) 1 - An overview of gas turbines. In: Boyce MP (ed) *Gas Turbine Engineering Handbook*, 4th edn. Butterworth-Heinemann, Oxford, pp 3–88. <https://doi.org/10.1016/B978-0-12-383842-1.00001-9>
6. Boyce MP (2012) 20 - Gas turbine performance test. In: Boyce MP (ed) *Gas Turbine Engineering Handbook*, 4th edn. Butterworth-Heinemann, Oxford, pp 769–802. <https://doi.org/10.1016/B978-0-12-383842-1.00020-2>
7. Choudhary T (2017) Novel and optimal integration of SOFC-ICGT hybrid cycle: energy analysis and entropy generation minimization. *Int J Hydrogen Energy* 42(23):15597–15612. <https://doi.org/10.1016/j.ijhydene.2017.04.277>
8. De Sa A, Al Zubaidy S (2011) Gas turbine performance at varying ambient temperature. *Appl Therm Eng* 31(14):2735–2739. <https://doi.org/10.1016/j.applthermaleng.2011.04.045>
9. Dincer I, Cengel YAJE (2001) Energy, entropy and exergy concepts and their roles in thermal engineering. *Entropy* 3(3):116–149
10. Ehyaei MA, Tahani M, Ahmadi P, Esfandiari M (2015) Optimization of fog inlet air cooling system for combined cycle power plants using genetic algorithm. *Appl Therm Eng* 76:449–461. <https://doi.org/10.1016/j.applthermaleng.2014.11.032>
11. Eke MN, Ozor PA, Aigbodion VS, Mbowa C (2021) Second law approach in the reduction of gas emission from gas turbine plant. *Fuel Commun* 9:100030. <https://doi.org/10.1016/j.jfueco.2021.100030>
12. Elberry MF, Elsayed AA, Teamah MA, Abdel-Rahman AA, Elsafty AF (2018) Performance improvement of power plants using absorption cooling system. *Alex Eng J* 57(4):2679–2686. <https://doi.org/10.1016/j.aej.2017.10.004>
13. Erdem HH, Sevilgen SH (2006) Case study: effect of ambient temperature on the electricity production and fuel consumption of a simple cycle gas turbine in Turkey. *Appl Therm Eng* 26(2):320–326. <https://doi.org/10.1016/j.applthermaleng.2005.08.002>
14. Fazeli A, Zandi S, Golbaten Mofrad K, Salehi G, Khoshgoftar Manesh MH, Shirmohammadi R (2022) Comparative thermo-economic optimization and exergoenvironmental analysis of an ejector refrigeration cycle integrated with a cogeneration system utilizing waste exhaust heat recovery. *Environ Prog Sustain Energy* 41(6):e13875. <https://doi.org/10.1002/ep.13875>
15. GilaniAhmed SI-u-HMSMS (2015) Solution crystallization detection for double-effect LiBr-H₂O steam absorption chiller. *Energy Procedia* 75:1522–1528. <https://doi.org/10.1016/j.egypro.2015.07.304>
16. Gomri R (2009) Second law comparison of single effect and double effect vapour absorption refrigeration systems. *Energy Convers Manage* 50(5):1279–1287. <https://doi.org/10.1016/j.enconman.2009.01.019>
17. Gomri R, Hakimi R (2008) Second law analysis of double effect vapour absorption cooler system. *Energy Convers Manage* 49(11):3343–3348. <https://doi.org/10.1016/j.enconman.2007.09.033>
18. Hu Y, Gao Y, Lv H, Xu G, Dong S (2018) A new integration system for natural gas combined cycle power plants with CO₂ capture and heat supply. *Energies* 11(11):3055
19. Kadam ST, Kyriakides A-S, Khan MS, Shehabi M, Papadopoulos AI, Hassan I, Rahman MA, Seferlis P (2022) Thermo-economic and environmental assessment of hybrid vapor

- compression-absorption refrigeration systems for district cooling. *Energy* 243:122991. <https://doi.org/10.1016/j.energy.2021.122991>
20. Kaushik SC, Arora A (2009) Energy and exergy analysis of single effect and series flow double effect water–lithium bromide absorption refrigeration systems. *Int J Refrig* 32(6):1247–1258. <https://doi.org/10.1016/j.ijrefrig.2009.01.017>
 21. Khan Y, Faruque MW, Nabil MH, Ehsan MM (2023) Ejector and vapor injection enhanced novel compression-absorption cascade refrigeration systems: a thermodynamic parametric and refrigerant analysis. *Energy Convers Manage* 289:117190. <https://doi.org/10.1016/j.enconman.2023.117190>
 22. Korakianitis T, Wilson D (1994) Models for predicting the performance of Brayton-cycle engines.
 23. Kumar S, Singh O (2013) Performance evaluation of gas-steam combined cycle having transpiration cooled gas turbine. *Distrib Gener Altern Energy J* 28(2):43–60. <https://doi.org/10.1080/21563306.2013.10677550>
 24. Kwon HM, Kim TS, Sohn JL, Kang DW (2018) Performance improvement of gas turbine combined cycle power plant by dual cooling of the inlet air and turbine coolant using an absorption chiller. *Energy* 163:1050–1061. <https://doi.org/10.1016/j.energy.2018.08.191>
 25. Lansing FL (1976) Computer modeling of a single-stage lithium bromide/water absorption refrigeration unit. Jet Propulsion Laboratory, California Institute of Technology, Pasadena, CA, Deep Space Network Progress Report. 42:247-57
 26. Matjanov E (2020) Gas turbine efficiency enhancement using absorption chiller Case study for Tashkent CHP. *Energy* 192:116625. <https://doi.org/10.1016/j.energy.2019.116625>
 27. Meraj M, Azhar M, Khan MZ, Salik Anjum MS, Sahil Faiz Ahmad M, Ab Rasheed MF, Iqbal Ahmed SI, Maqbul Alam MN (2021) Thermal modelling of PVT-CPC integrated vapour absorption refrigeration system. *Mater Today: Proc* 38:391–396. <https://doi.org/10.1016/j.matpr.2020.07.547>
 28. Midilli A, Dincer I (2009) Development of some exergetic parameters for PEM fuel cells for measuring environmental impact and sustainability. *Int J Hydrogen Energy* 34(9):3858–3872. <https://doi.org/10.1016/j.ijhydene.2009.02.066>
 29. Mohapatra AK (2014) Thermodynamic assessment of impact of inlet air cooling techniques on gas turbine and combined cycle performance. *Energy* 68:191–203. <https://doi.org/10.1016/j.energy.2014.02.066>
 30. Mohapatra AK (2015) Comparative analysis of inlet air cooling techniques integrated to cooled gas turbine plant. *J Energy Inst* 88(3):344–358. <https://doi.org/10.1016/j.joei.2014.07.006>
 31. Mohapatra AK (2018) Exergetic evaluation of gas-turbine based combined cycle system with vapor absorption inlet cooling. *Appl Therm Eng* 136:431–443. <https://doi.org/10.1016/j.applthermaleng.2018.03.023>
 32. Nag P (2002) Power plant engineering. Tata McGraw-Hill Education, New York
 33. Pátek J, Klomfar J (2006) A computationally effective formulation of the thermodynamic properties of LiBr–H₂O solutions from 273 to 500K over full composition range. *Int J Refrig* 29(4):566–578. <https://doi.org/10.1016/j.ijrefrig.2005.10.007>
 34. Rai J, Hasan N, Arora B, Garai R, Kapoor R (2013) Performance analysis of CCGT power plant using MATLAB/Simulink based simulation. *Int J Adv Res Technol* 2:285–290
 35. Redko A, Redko O, DiPippo R (2020) 1–Principles and operation of refrigeration and heat pump systems. In: Redko A, Redko O, DiPippo R (eds) *Low-Temperature Energy Systems with Applications of Renewable Energy*. Academic Press, pp 1–45. <https://doi.org/10.1016/B978-0-12-816249-1.00001-7>
 36. Ren J, Qian Z, Yao Z, Gan N, Zhang Y (2019) Thermodynamic evaluation of LiCl–H₂O and LiBr–H₂O absorption refrigeration systems based on a novel model and algorithm. *Energies* 12(15):3037
 37. Shukla AK, Singh O (2017) Thermodynamic investigation of parameters affecting the execution of steam injected cooled gas turbine based combined cycle power plant with vapor absorption inlet air cooling. *Appl Therm Eng* 122:380–388. <https://doi.org/10.1016/j.applthermaleng.2017.05.034>
 38. Singh OK (2016) Performance enhancement of combined cycle power plant using inlet air cooling by exhaust heat operated ammonia-water absorption refrigeration system. *Appl Energy* 180:867–879. <https://doi.org/10.1016/j.apenergy.2016.08.042>
 39. Sinha AA, Choudhary T, Ansari MZ (2023) Estimation of exergy-based sustainability index and performance evaluation of a novel intercooled hybrid gas turbine system. *Int J Hydrogen Energy* 48(23):8629–8644. <https://doi.org/10.1016/j.ijhydene.2022.10.260>
 40. Sinha AA, Saini G, Sanjay SAK, Ansari MZ, Dwivedi G, Choudhary T (2023) A novel comparison of energy-exergy, and sustainability analysis for biomass-fueled solid oxide fuel cell integrated gas turbine hybrid configuration. *Energy Convers Manage* 283:116923. <https://doi.org/10.1016/j.enconman.2023.116923>
 41. Sinha AA, Sanjay AMZ, Shukla AK, Choudhary T (2023) Comprehensive review on integration strategies and numerical modeling of fuel cell hybrid system for power and heat production. *Int J Hydrogen Energy* 48(86):33669–33704. <https://doi.org/10.1016/j.ijhydene.2023.05.097>
 42. Talukdar K, Gogoi TK (2016) Exergy analysis of a combined vapor power cycle and boiler flue gas driven double effect water–LiBr absorption refrigeration system. *Energy Convers Manage* 108:468–477. <https://doi.org/10.1016/j.enconman.2015.11.020>
 43. Touloukian YS, Tadayas M (1970) Thermo-physical Properties of Matter. IFI/PLENUM, Washington
 44. Vandervort C, Leach D, Walker D, Sasser J Commercialization and Fleet Experience of the 7/9HA Gas Turbine Combined Cycle. In: *Turbo Expo: Power for Land, Sea, and Air, 2019*. American Society of Mechanical Engineers, p V003T008A006
 45. Yin H, Qu M, Archer DH (2010) Model based experimental performance analysis of a microscale LiBr–H₂O steam-driven double-effect absorption Chiller. *Appl Therm Eng* 30(13):1741–1750. <https://doi.org/10.1016/j.applthermaleng.2010.04.004>

Publisher's Note Springer Nature remains neutral with regard to jurisdictional claims in published maps and institutional affiliations.

Springer Nature or its licensor (e.g. a society or other partner) holds exclusive rights to this article under a publishing agreement with the author(s) or other rightsholder(s); author self-archiving of the accepted manuscript version of this article is solely governed by the terms of such publishing agreement and applicable law.